

A minimized fluorescent chemosensor array utilizing carboxylate-attached polythiophenes on a chip for metal ions detection

Yui Sasaki, Xiaojun Lyu, Zhoujie Zhang, Tsuyoshi Minami (✉)

Institute of Industrial Science, The University of Tokyo, Tokyo 153-8505, Japan

© Higher Education Press 2021

Abstract Chemosensor arrays have a great potential for on-site applications in real-world scenarios. However, to fabricate on chemosensor array a number of chemosensors are required to obtain various optical patterns for multi-analyte detection. Herein, we propose a minimized chemosensor array composed of only two types of carboxylate-functionalized polythiophene derivatives for the detection of eight types of metal ions. Upon recognition of the metal ions, the polythiophenes exhibited changes in their fluorescence intensity and various spectral shifts. Although both chemosensors have the same polymer backbone and recognition moiety, only the difference in the number of methylene groups contributed to the difference in the fluorescence response patterns. Consequently, the metal ions in aqueous media were successfully discriminated qualitatively and quantitatively by the chemosensor microarray on the glass chip. This study offers an approach for achieving a minimized chemosensor array just by changing the alkyl chain lengths without the necessity for many receptors and reporters.

Keywords metal ions, polythiophene, chemosensor array, fluorescence, pattern recognition

1 Introduction

Chemosensor arrays offer accurate and rapid detection of diverse analytes by the combination with versatile colorful sensor elements [1–4]. To date, various types of small molecule- [5,6] or polymer- [7–9] based chemosensor arrays have been developed for multi-analyte detection. Among them, π -conjugated polymer-based chemosensors are some of the more important candidates for array applications owing to their unique optical properties

[10,11]. Their optical responses are keenly affected by the inter- and intramolecular interactions stemmed from molecular recognition phenomena. Thus, π -conjugated polymer-based chemosensors, such as poly(*p*-phenyleneethynylene)s (PPEs) [12], allow not only the visualization of molecular recognition at the side chains but also the amplification of the sensitivity due to molecular wire effects [11]. For example, Miranda et al. reported water-soluble PPEs for proteins detection. The PPEs with six types of charged or neutral side chains offered different optical response patterns, which allowed the discrimination of seventeen types of proteins [13].

Regardless of small molecule- [14,15] and polymer-based chemosensors [16], various types of chemosensors are generally required even in an array to obtain optical response patterns for multi-analyte detection. To avoid synthetic burdens and complicated fabrication processes, the arrays should be constructed by a small number of chemosensors. Examples for the small molecule-type minimized chemosensor arrays have been previously reported [17–25], while the minimization of the polymer-based chemosensors have rarely been attempted [26,27]. For the polymer-based chemosensors, the reduction of the number of the chemosensors is generally limited by the difficulties for simple tuning of the color patterns using the same rigid backbones. To overcome this potential drawback, we focused on polythiophene derivatives (PTs) as chemosensors [28–37]. Owing to their relatively flexible backbones, PT derivatives allow fine-tuning of their optical properties for the chemosensor arrays. This feature arises from the co-planarization of the thiophene units and subsequent self-aggregation which are induced by molecular recognition phenomena [30,33]. We herein report the simultaneous detection of various types of metal ions (Al^{3+} , Ca^{2+} , Cd^{2+} , Co^{2+} , Cu^{2+} , Ni^{2+} , Pb^{2+} , Zn^{2+}) using a chemosensor array composed of only two types of the carboxylate-functionalized PT derivatives (Fig. 1). Some of the metal ions are beneficial for maintaining the health

of organisms. However, the over-accumulation of the essential metal ions or uptake of toxic ones causes various adverse effects [38]. Thus, the simultaneous detection of metal ions is of significance to avoid environmental and physiological concerns [39–43]. The carboxy groups at the side chains of the PT derivatives were employed as coordination sites for the metal ions [30]. The coordination of the metal ions to the functional group resulted in various changes in the optical properties (i.e., intensity changes and spectral shifts) of PT derivatives, which allowed us to prepare the minimized chemosensor array. The array was finally fabricated on a small glass chip from the viewpoint of on-site detection. Notably, the glass chip combined with analyses by a charge coupled device (CCD) camera and image processing [33] enabled the simultaneous detection of the eight types of metal ions. Thus, the PT-based chemosensor array is one-step forward toward achieving miniaturized chemosensor arrays.

2 Experimental

2.1 Materials

Reagents and solvents were purchased from commercial suppliers and used as received. For the optical titrations of metal ions, copper(II) perchlorate hexahydrate, cobalt(II) perchlorate hexahydrate, nickel(II) perchlorate hexahy-

drate, zinc(II) perchlorate hexahydrate, mercury(II) perchlorate hydrate, calcium perchlorate tetrahydrate, cadmium(II) perchlorate hydrate, aluminum(III) perchlorate nonahydrate, lead(II) perchlorate hydrate, lithium perchlorate, manganese(II) perchlorate hydrate, palladium(II) nitrate, and chromium(III) nitrate nonahydrate were purchased from Sigma-Aldrich Co. LLC. PT derivatives, poly[3-(5-carboxybutyl)thiophene-2,5-diyl] (**1**) ($M_w = 3.0 \times 10^4$ – 4.0×10^4 g·mol⁻¹) and poly[3-(6-carboxylpentyl)thiophene-2,5-diyl] (**2**) ($M_w = 5.5 \times 10^4$ – 6.5×10^4 g·mol⁻¹) were purchased from Rieke Metals, Inc. NaCl, 4-(2-hydroxyethyl)-1-piperazineethanesulfonic acid (HEPES), disodium hydrogenphosphate dodecahydrate, and dimethyl sulfoxide (DMSO) were purchased from Kanto Chemical Co. Inc. A hydrogel matrix (model: HydroMed D4) for the array experiment was purchased from AdvanSource Biomaterials Corp. Aqueous solutions for all experiments were prepared using Mill-Q water (18.2 M Ω ·cm⁻¹).

2.2 Measurements

UV-vis spectra were measured using a SHIMADZU UV-2600 double-beam spectrophotometer, within the wavelength range of 300–800 nm. Fluorescence responses were measured by a HITACHI F-7100 spectrophotometer. Both **1** (15 $\mu\text{mol}\cdot\text{L}^{-1}\cdot\text{unit}^{-1}$) and **2** (10 $\mu\text{mol}\cdot\text{L}^{-1}\cdot\text{unit}^{-1}$) were excited at 480 nm, and the fluorescence spectra were

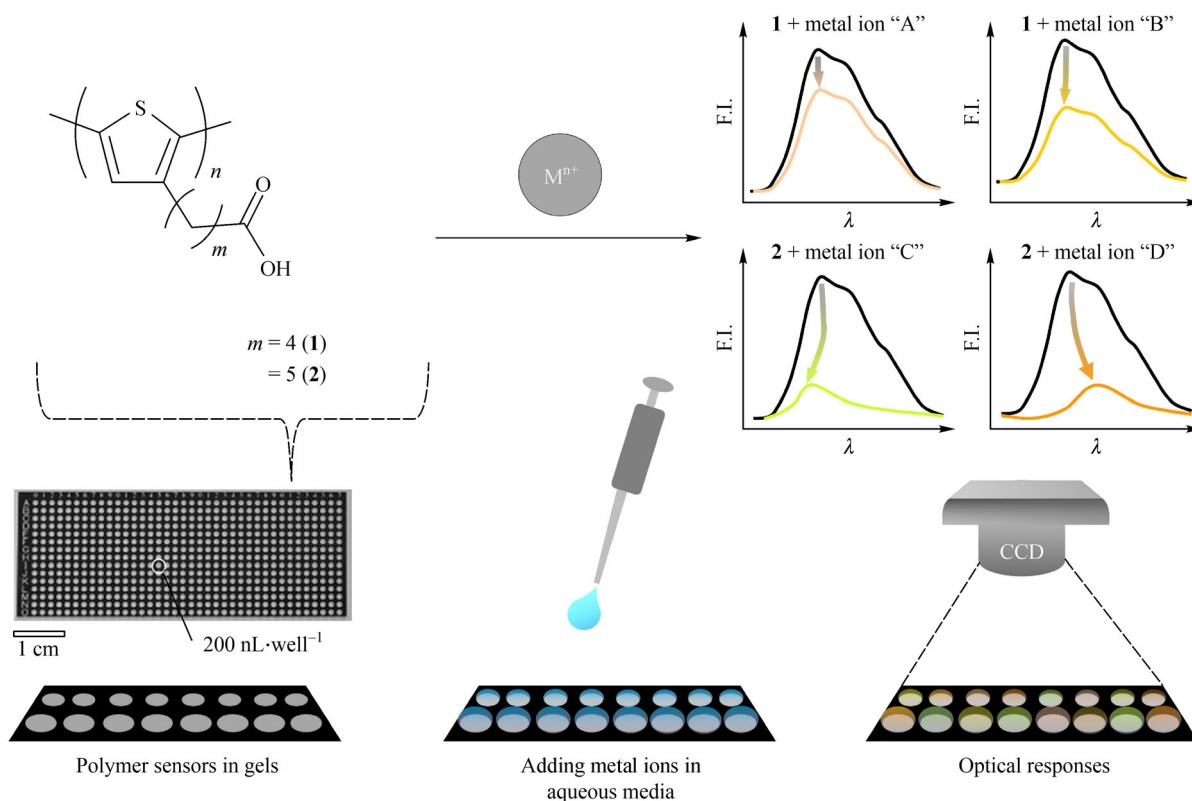


Fig. 1 Schematic illustration of the polythiophene-based minimized chemosensor array on the glass chip for the simultaneous detection of metal ions.

recorded within the wavelength range from 500–800 nm at the scanning rate of $240 \text{ nm} \cdot \text{min}^{-1}$. Titration isotherms were prepared by plotting the fluorescence maxima at 594 and 610 nm for **1** and **2**, respectively. Both optical measurements were conducted under ambient room conditions at $25 \text{ }^\circ\text{C}$. The absolute quantum yields (Table S1, cf. Electronic Supplementary Material, ESM) were measured using an absolute photoluminescence quantum yield spectrometer (Hamamatsu Photonics Quantaaurus-QY, C11347-01). The lifetimes of the fluorophores (Table S1) were recorded on a fluorescence lifetime spectrometer (Hamamatsu Photonics Quantaaurus-Tau, C11367-01). A quartz cuvette (Hamamatsu Photonics A10095-02, $10 \text{ mm} \times 10 \text{ mm}$) was used for each measurement.

2.3 Array experiment

The fluorescent sensor **1** or **2** ($250 \text{ } \mu\text{mol} \cdot \text{L}^{-1}$) and HydroMed D4 (3.6 wt-%) were mixed in a HEPES buffer ($50 \text{ mmol} \cdot \text{L}^{-1}$) containing NaCl ($10 \text{ mmol} \cdot \text{L}^{-1}$), and the pH value was adjusted to 7.4. The solutions were dispensed into a 405-microwell glass chip at $0.2 \text{ } \mu\text{L}$ per well utilizing a robotic dispenser system (IMAGEMASTER 350, Musashi Engineering). The glass chip was dried in vacuo at $45 \text{ }^\circ\text{C}$ for 5 min. Next, a HEPES buffer solution (pH 7.4) was pipetted to the glass chip at $0.2 \text{ } \mu\text{L}$ per well and the glass chip was dried again. The light-emission of the fabricated fluorescence sensor chip at this step was recorded by an imaging scanner (Anatech, FluoroPhoreStar3000). Finally, the target metal ions in the HEPES buffer solutions were pipetted into the glass chip at the same volume and treated by drying process, followed by image recording. The datasets of the fluorescence images were obtained by the following combinations of the light sources and the color filters: λ_{ex} (375 nm)– λ_{em} ($450 \pm 40 \text{ nm}$ band path (BP)), λ_{ex} (375 nm)– λ_{em} (530 nm long path (LP)), λ_{ex} (375 nm)– λ_{em} ($540 \pm 50 \text{ nm}$ BP), λ_{ex} (375 nm)– λ_{em} (580 nm LP), λ_{ex} (375 nm)– λ_{em} (630 nm LP), λ_{ex} (470 nm)– λ_{em} (530 nm LP), λ_{ex} (470 nm)– λ_{em} (580 nm LP), λ_{ex} (470 nm)– λ_{em} (630 nm LP), λ_{ex} (470 nm)– λ_{em} ($700 \pm 35 \text{ nm}$ BP), λ_{ex} (530 nm)– λ_{em} (580 nm LP), λ_{ex} (530 nm)– λ_{em} (630 nm LP) and λ_{ex} (530 nm)– λ_{em} ($700 \pm 35 \text{ nm}$ BP) (Table S2, cf. ESM). The obtained images were analyzed by ImageJ. The data extraction was carried out with twenty-eight repetitions. The obtained data for the qualitative assay were analyzed by a linear discriminant analysis (LDA) [1,2]. A leave-one-out cross-validation protocol was employed to determine the classification rate.

3 Results and discussion

3.1 Metal-ion titration using spectroscopic methods

Among the PTs ($m = 3\text{--}6$), the *n*-butyl carboxylate- and *n*-

pentyl carboxylate-functionalized PTs ($m = 4, 5$) (**1** and **2**) were employed for the simultaneous detection of the metal ions. In this study, the appropriate alkyl chain length was selected to avoid undesirable effects of PT derivatives with short and long carboxy alkyl groups on the sensing properties. The short one ($m = 3$) caused a doping effect on PTs [44], while the aggregation behavior was observed for the long alkyl chain ($m = 6$) in polar solvents [45]. Thus, only two polymer-based sensors were utilized for the optical investigations. First, the coordination of the metal ions on the carboxy group was monitored by UV-vis spectrophotometry. The representative result of the UV-vis titration is shown in Fig. 2. The addition of Cu^{2+} resulted in a clear change of the spectrum of **2** with the redshift of the absorption maximum from 476 to 550 nm, indicating the co-planarization of the thiophene units stemmed from the recognition of Cu^{2+} [28–37]. Moreover, the slight increase in the baseline absorption reflects the aggregation of the PT, which is most probably due to Rayleigh scattering [35,45,46]. Thus, the spectral changes demonstrated the molecular behavior of the PT induced by the recognition of the metal ions.

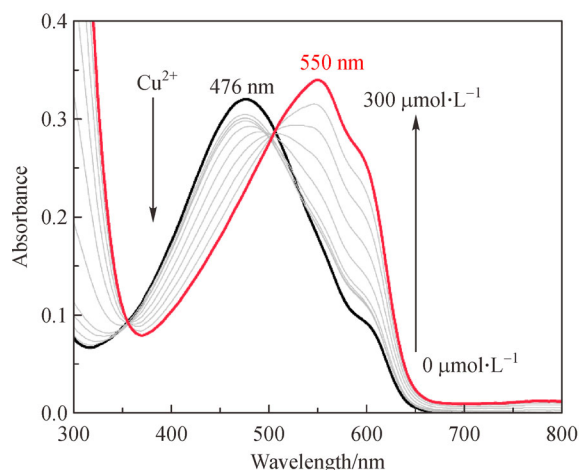


Fig. 2 UV-vis spectra of **2** ($100 \text{ } \mu\text{mol} \cdot \text{L}^{-1}$) upon increasing the concentration of Cu^{2+} in DMSO at $25 \text{ }^\circ\text{C}$ ($[\text{Cu}^{2+}] = 0\text{--}300 \text{ } \mu\text{mol} \cdot \text{L}^{-1}$). The spectra were recorded in 10 min after mixing **2** and Cu^{2+} .

The addition of Cu^{2+} also affected the fluorescence properties of **2**, as shown in Fig. 3. The fluorescence intensity of **2** decreased and blue-shifted ($\Delta\lambda = 20 \text{ nm}$) upon the addition of Cu^{2+} . The fluorescence spectral change was probably induced by multiple factors including spin-orbit coupling, and changes in planarity and the aggregate state [47,48]. The titration isotherm allowed to estimate the Stern-Volmer quenching constant (K_{sv}) [49] of $2.1 \times 10^8 \text{ L} \cdot \text{mol}^{-1}$ for Cu^{2+} . In addition, the Al^{3+} ion as well as the Cu^{2+} ion induced a gradual decrease in the fluorescence intensity, while the emission wavelength of **2** was redshifted ($\Delta\lambda = 24 \text{ nm}$) in contrast to that of the Cu^{2+}

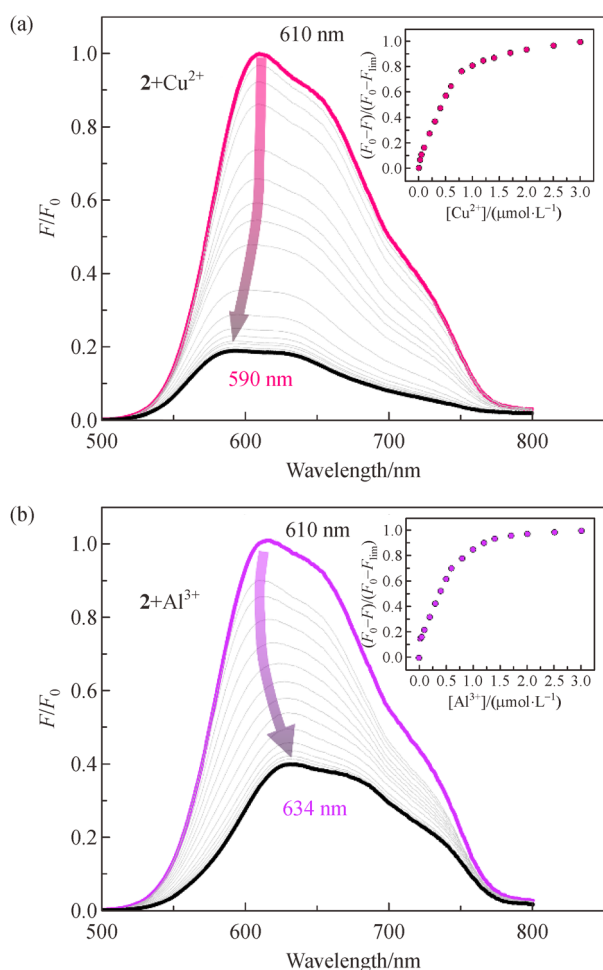


Fig. 3 Fluorescence spectra of **2** upon increasing the concentrations of (a) Cu^{2+} and (b) Al^{3+} in DMSO at $25\text{ }^{\circ}\text{C}$ ($[\text{Metal ion}] = 0\text{--}3.0\ \mu\text{mol}\cdot\text{L}^{-1}$, $\lambda_{\text{ex}} = 480\ \text{nm}$). The spectra were recorded in 10 min after mixing **2** and the metal ions. Insets: the titration isotherms obtained by plotting the maximum emission intensities ($\lambda_{\text{em}} = 610\ \text{nm}$) at each concentration of the metal ions).

ion. The K_{sv} value for the Al^{3+} ion was estimated to be $2.6 \times 10^8\ \text{L}\cdot\text{mol}^{-1}$. The significant quenching is probably due to an efficient interchain aggregation by the trivalent ion [50,51]. More importantly, the alkyl chain length also contributes to the fluorescence response patterns. As examples of the comparative measurement with the same metal ion but different alkyl chain lengths, Fig. 4 shows the fluorescence characteristics of **1** and **2** with an increase in Zn^{2+} concentrations. Remarkably, the fluorescence intensity of **2** drastically decreased resulting in a relatively large K_{sv} value ($1.1 \times 10^8\ \text{L}\cdot\text{mol}^{-1}$), whereas that of **1** was almost unaffected.

To further investigate the selectivity of the polymer-based chemosensors, the fluorescence titrations were performed with the total eight types of metal ions. Several metal ions (Hg^{2+} , Cr^{3+} , Mn^{2+} , Pd^{2+} , Li^{+} , and Na^{+}) were

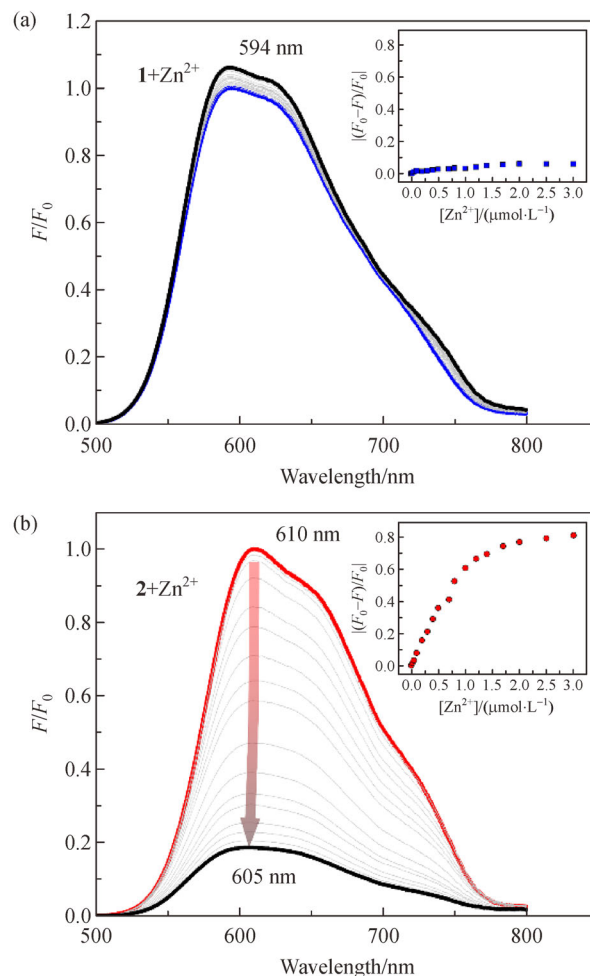


Fig. 4 Fluorescence spectra of (a) **1** and (b) **2** upon increasing the concentrations of Zn^{2+} in DMSO at $25\text{ }^{\circ}\text{C}$ ($[\text{Zn}^{2+}] = 0\text{--}3.0\ \mu\text{mol}\cdot\text{L}^{-1}$, $\lambda_{\text{ex}} = 480\ \text{nm}$). The spectra were recorded in 10 min after mixing **1** or **2** and the metal ions. Insets: the titration isotherms obtained by plotting the maximum emission intensities at $594\ \text{nm}$ and $610\ \text{nm}$ for **1** and **2**, respectively).

excluded from the list of the analytes due to their little or no influences on the fluorescence changes. PT derivatives **1** and **2** responded to the other types of metal ions, showing moderate selectivity along with different binding affinities (Fig. 5 and Table 1). The PT **2** tended to exhibit higher apparent binding constants for the metal ions compared to those of **1** (Table 1), which could presumably be attributed to the stabilized coordination complex by the long alkyl chain [52]. Indeed, a previous report regarding a statistical analysis (i.e., analysis of variance) of PT chemosensors implied the significance of the length of alkyl chains [33]. The flexibility derived from the long alkyl chain ($m = 5$) could contribute to the favorable complexation with analytes, resulting in larger optical changes. In addition, the limit of detection was estimated to be in the ppb ($\times 10^{-9}$)–sub-ppm ($\times 10^{-6}$) levels based on the IUPAC

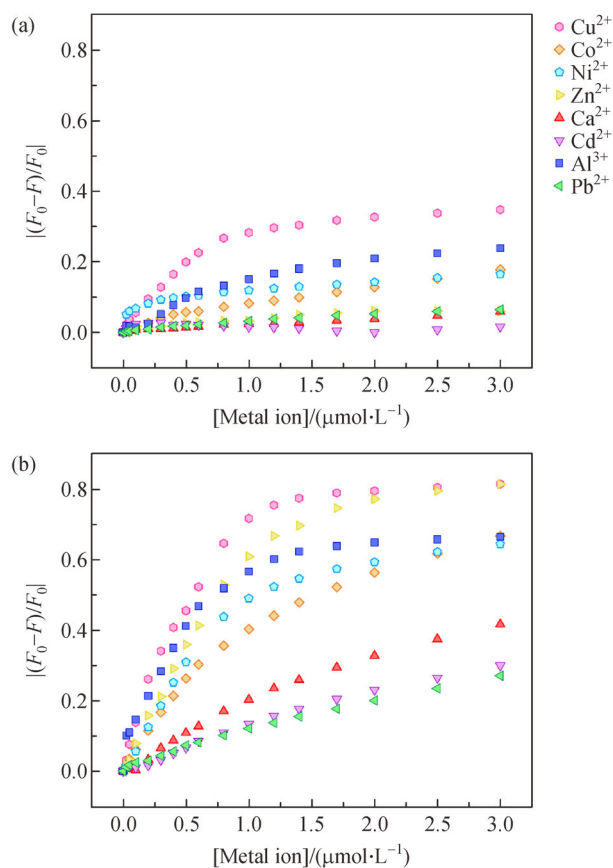


Fig. 5 Response selectivity of (a) **1** and (b) **2** for the metal ions (Each titration isotherm was obtained by plotting the maximum emission intensities (λ_{ex} at 594 nm and 610 nm for **1** and **2**, respectively) at each concentration of the metal ions. $\lambda_{\text{ex}} = 480$ nm).

Table 1 The Stern-Volmer quenching constants of **1** and **2** ($K_{\text{sv}}/(\text{L} \cdot \text{mol}^{-1})$)

Metal ions	1	2
Cu^{2+}	2.0×10^8	2.1×10^8
Al^{3+}	7.1×10^7	2.6×10^8
Ca^{2+}	1.6×10^7	2.7×10^7
Cd^{2+}	N.D. ^{a)}	2.3×10^7
Co^{2+}	3.7×10^7	7.8×10^7
Ni^{2+}	1.3×10^8	1.3×10^8
Pb^{2+}	4.0×10^7	2.4×10^7
Zn^{2+}	$< 10^3$	1.1×10^8

a) N.D.: not determined due to the small response.

rule (i.e., the 3σ method) (Table S2) [53]. As demonstrated herein, the diverse response patterns (i.e., shifts of emission wavelengths and fluorescence intensity changes) were obtained with the same polymer backbone depending on the metal ion species and the alkyl chain lengths. Furthermore, the coordination number and the geometry of each metal ion species presumably affected the binding constants determined [52]. Such distinct optical contrast

plays significant roles in increasing the number of datasets for pattern recognition of the minimized chemosensor array, which would allow the accurate and simultaneous discrimination of the metal ions.

3.2 Array experiment

To achieve a robust and easy-to-detect sensor array system, a hydrogel-based microarray was employed. Hydrogels are known to prevent self-aggregation of chemosensors in the solid state [54,55]. In addition, the water-soluble polymer materials absorb aqueous samples with high efficiency [54]. More importantly, the analyte detection can be achieved in aqueous media even using poorly water-soluble chemosensors. The 405-well microarray chip was injected with **1** or **2** in a polyurethane gel using the robotic dispenser. Subsequently, each metal ion ($10 \mu\text{mol} \cdot \text{L}^{-1}$) dissolved in the HEPES buffer solution ($50 \text{mmol} \cdot \text{L}^{-1}$) containing NaCl ($10 \text{mmol} \cdot \text{L}^{-1}$) was added to the wells. To record the fluorescence patterns of the microchip, the CCD camera was utilized with three light sources (i.e., UV, blue and green) and six color filters. The combination of the light sources and the color filters provided red, green and blue variations for the image data analysis. Indeed, a heatmap of the microchip displayed a fingerprint-like response pattern upon the recognition of metal ions (Fig. 6).

A qualitative analysis was carried out for the simultaneous discrimination of the metal ions in the aqueous media. The obtained dataset was analyzed by LDA with the jack knife method. As shown in Fig. 7, the LDA canonical score plots showed the accurate discrimination of the eight types of metal ions with 100% correct classification. In comparison with the cluster for control, the positions of the

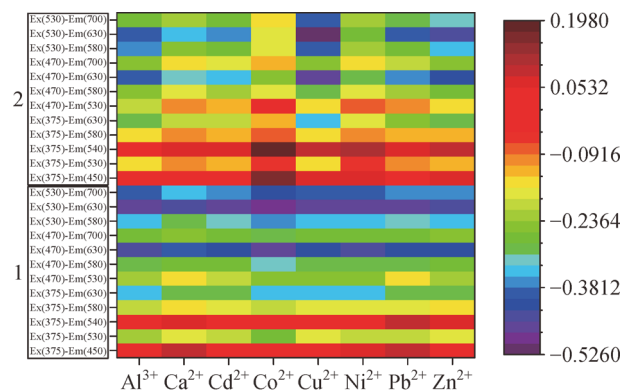


Fig. 6 Heat map of the microchip containing **1** or **2** in the presence of the metal ions (The fluorescence response patterns were obtained by the combination of three types of light sources (i.e., $\lambda_{\text{ex}} = 375, 470,$ and 530 nm) and six types of CCD camera filters (i.e., $\lambda_{\text{em}} = 450, 530, 540, 580, 630,$ and 700 nm). $[\text{Hydrogel}] = 3.6 \text{ wt}\%$, $[\mathbf{1}] = [\mathbf{2}] = 250 \mu\text{mol} \cdot \text{L}^{-1} \cdot \text{unit}^{-1}$. $[\text{Metal ion}] = 10 \mu\text{mol} \cdot \text{L}^{-1}$ in a HEPES buffer ($50 \text{mmol} \cdot \text{L}^{-1}$) with NaCl ($10 \text{mmol} \cdot \text{L}^{-1}$) at pH 7.4).

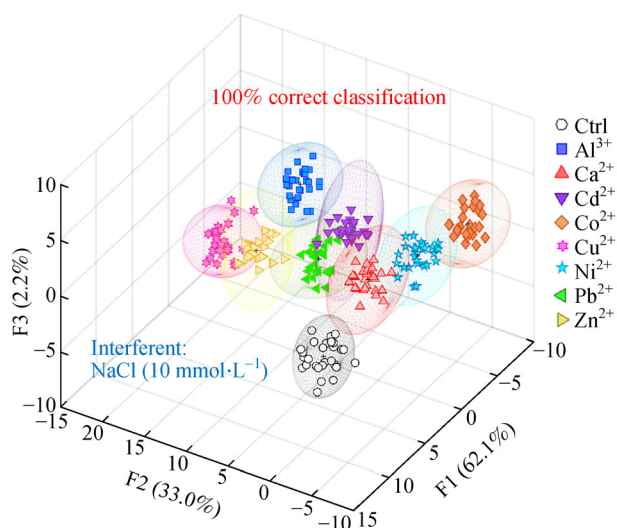


Fig. 7 LDA canonical score plots with 99% confidence ellipsoids for the qualitative analysis of the eight types of the metal ions in a HEPES buffer ($50 \text{ mmol}\cdot\text{L}^{-1}$) with NaCl ($10 \text{ mmol}\cdot\text{L}^{-1}$) at pH 7.4 (For each trial, twenty-eight repetitions were conducted. $[\text{Hydrogel}] = 3.6 \text{ wt}\%$, $[\mathbf{1}] = [\mathbf{2}] = 250 \text{ }\mu\text{mol}\cdot\text{L}^{-1}\cdot\text{unit}^{-1}$. $[\text{Metal ion}] = 10 \text{ }\mu\text{mol}\cdot\text{L}^{-1}$).

clusters of the metal ions reflect the turn-off responses of PT derivatives. For example, the distance between the cluster of Cu^{2+} and the control was far more than that between others, which corresponded to the increased fluorescence responses along with a higher K_{sv} value. In contrast to that for Cu^{2+} , the distance between Ca^{2+} and the control was closer due to the low K_{sv} value. Furthermore, the relatively large response space (F1: 62.1%, F2: 33.0%, and F3: 2.2%) despite using only the two chemosensors suggests that the successful classification is a result of the diverse optical response patterns offered by the PT backbones.

Furthermore, we conducted a semi-quantitative and quantitative analysis in the mixtures. In these assays, a combination of Cu^{2+} and Al^{3+} was employed as the target metal ions. Since the combination causes a reduction in the chlorophyll content and the inhibition of plant growth and respiration, the simultaneous detection of Cu^{2+} and Al^{3+} is important from the viewpoint of environmental and agricultural fields [56]. The result of the semi-quantitative analysis in Fig. 8 shows the distribution of the clusters depending on the concentrations of the two metal ions. Finally, the quantitative analysis was carried out using a support vector machine (SVM). SVM includes two groups: the first group (black squares in Fig. 9) for the establishment of the calibration model and the second group for the prediction model (red circle). The result of the quantitative analysis offered a successful prediction of the unknown concentrations of the two metal ion species, demonstrating the potential utility of the proposed chemosensors (Fig. 9). In addition, the limits of detection [53] for Cu^{2+} and Al^{3+} were estimated as 0.2 and 0.03 ppm, respectively.

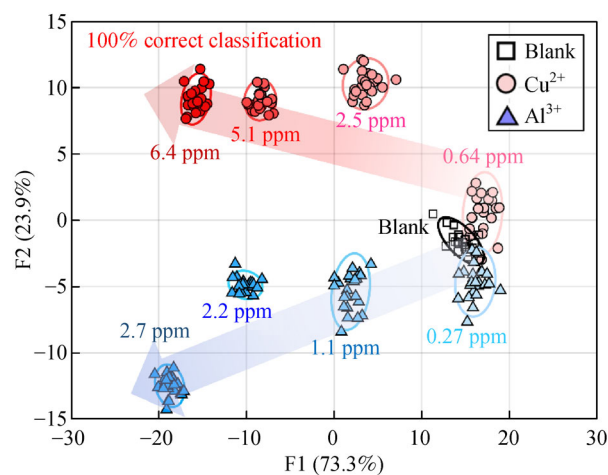


Fig. 8 The LDA canonical score plots for the semi-quantitative analysis of Cu^{2+} and Al^{3+} in the presence of NaCl ($10 \text{ mmol}\cdot\text{L}^{-1}$) (The ellipsoids indicate 99% confidence).

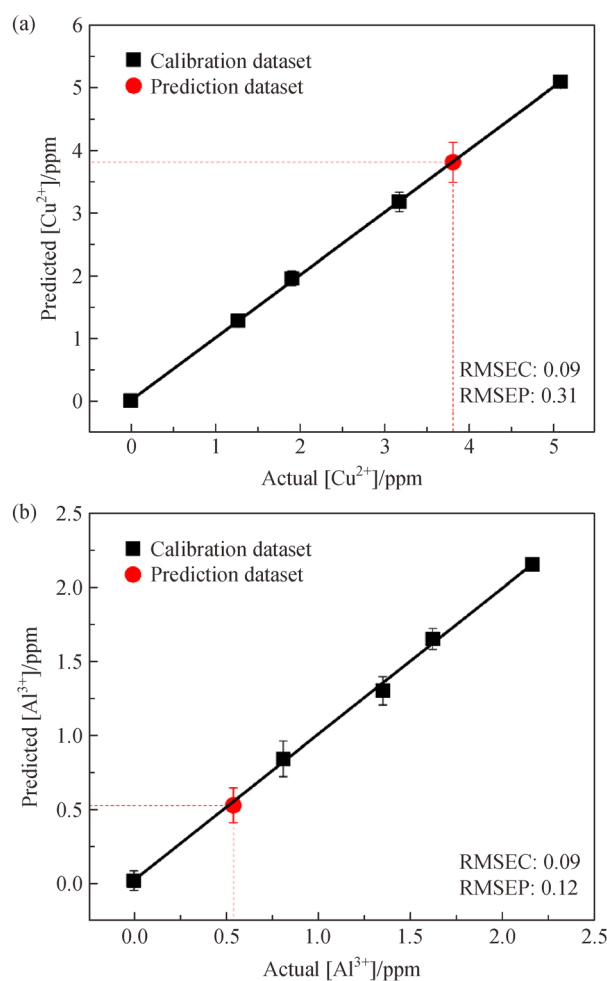


Fig. 9 Quantitative analysis of (a) Cu^{2+} and (b) Al^{3+} in the mixture containing NaCl ($10 \text{ mmol}\cdot\text{L}^{-1}$) using SVM (The values of the root-mean-square error of calibration and prediction attest the high accuracy of the analyses).

4 Conclusions

In this study, we fabricated a fluorescence-based chemosensor array for metal-ion detection utilizing only two types of carboxylate-functionalized PTs. Interestingly, the selectivity of the PTs reflected the difference in the alkyl chain lengths and the type of metal ions. Furthermore, the flexibility of the PT backbones contributed to the diverse spectral changes to generate numerous optical response patterns, resulting in the fluorescence fingerprint-like response patterns for the fabricated microarray chip. The result of LDA plots confirmed the accurate classification of the eight metal ions by the image analysis. The most interesting point is that only one difference in the number of methylene groups of the same type of chemosensor contributed to the diverse optical response patterns for the discrimination of the metal ion species. In other words, this study provides an easy approach for achieving minimized chemosensor arrays by changing the spacer unit (i.e., the alkyl chain length) without gathering various reporters and receptors, which would facilitate the application of the arrays in real-world scenarios.

Acknowledgements Tsuyoshi Minami thanks JSPS KAKENHI (Grant No. JP20K21204) and JST CREST (Grant No. JPMJCR2011). Yui Sasaki thanks JSPS KAKENHI (Grant No. JP18J21190). We also thank Dr. Shin-ya Takizawa of the University of Tokyo for the measurements of emission quantum yield and lifetime.

Electronic Supplementary Material Supplementary material is available in the online version of this article at <http://dx.doi.org/10.1007/s11705-021-2037-y> and is accessible for authorized users.

References

1. Anzenbacher P Jr, Lubal P, Buček P, Palacios M A, Kozelkova M E. A practical approach to optical cross-reactive sensor arrays. *Chemical Society Reviews*, 2010, 39(10): 3954–3979
2. Li Z, Askim J R, Suslick K S. The optoelectronic nose: colorimetric and fluorometric sensor arrays. *Chemical Reviews*, 2019, 119(1): 231–292
3. Diehl K L, Anslyn E V. Array sensing using optical methods for detection of chemical and biological hazards. *Chemical Society Reviews*, 2013, 42(22): 8596–8611
4. Sasaki Y, Kubota R, Minami T. Molecular self-assembled chemosensors and their arrays. *Coordination Chemistry Reviews*, 2021, 429: 213607
5. Smith D G, Topolnicki I L, Zwicker V E, Jolliffe K A, New E J. Fluorescent sensing arrays for cations and anions. *Analyst*, 2017, 142(19): 3549–3563
6. Lavigne J J, Anslyn E V. Sensing a paradigm shift in the field of molecular recognition: from selective to differential receptors. *Angewandte Chemie International Edition*, 2001, 40(17): 3118–3130
7. Geng Y, Peveler W J, Rotello V M. Array-based “chemical nose” sensing in diagnostics and drug discovery. *Angewandte Chemie International Edition*, 2019, 58(16): 5190–5200
8. Shimizu K D, Stephenson C J. Molecularly imprinted polymer sensor arrays. *Current Opinion in Chemical Biology*, 2010, 14(6): 743–750
9. Ikeda M, Ochi R, Hamachi I. Supramolecular hydrogel-based protein and chemosensor array. *Lab on a Chip*, 2010, 10(24): 3325–3334
10. Lemieux É J, Leclerc M. *Conjugated Polyelectrolytes: Fundamentals and Applications*. New Jersey: Wiley-VCH Weinheim, 2013, 231–261
11. McQuade D T, Pullen A E, Swager T M. Conjugated polymer-based chemical sensors. *Chemical Reviews*, 2000, 100(7): 2537–2574
12. Bunz U H F. Poly(*p*-phenyleneethynylene)s by alkyne metathesis. *Accounts of Chemical Research*, 2001, 34(12): 998–1010
13. Miranda O R, You C C, Phillips R, Kim I B, Ghosh P S, Bunz U H F, Rotello V M. Array-based sensing of proteins using conjugated polymers. *Journal of the American Chemical Society*, 2007, 129(32): 9856–9857
14. Rhee H W, Lee S W, Lee J S, Chang Y T, Hong J I. Focused fluorescent probe library for metal cations and biological anions. *ACS Combinatorial Science*, 2013, 15(9): 483–490
15. Ihde M H, Pridmore C F, Bonizzoni M. Pattern-based recognition systems: overcoming the problem of mixtures. *Analytical Chemistry*, 2020, 92(24): 16213–16220
16. Han J, Wang B, Bender M, Seehafer K, Bunz U H F. Water-soluble poly(*p*-aryleneethynylene)s: a sensor array discriminates aromatic carboxylic acids. *ACS Applied Materials & Interfaces*, 2016, 8(31): 20415–20421
17. Sasaki Y, Kojima S, Hamedpour V, Kubota R, Takizawa S, Yoshikawa I, Houjou H, Kubo Y, Minami T. Accurate chiral pattern recognition for amines from just a single chemosensor. *Chemical Science*, 2020, 11(15): 3790–3796
18. Cao Z, Cao Y, Kubota R, Sasaki Y, Asano K, Lyu X, Zhang Z, Zhou Q, Zhao X, Xu X, Wu S, Minami T, Liu Y. Fluorescence anion chemosensor array based on pyrenylboronic acid. *Frontiers in Chemistry*, 2020, 8: 414
19. Cao Y, Zhang L, Huang X, Xin Y, Ding L. Discrimination of metalloproteins by a mini sensor array based on bispyrene fluorophore/surfactant aggregate ensembles. *ACS Applied Materials & Interfaces*, 2016, 8(51): 35650–35659
20. Anzenbacher P Jr, Liu Y, Palacios M A, Minami T, Wang Z, Nishiyabu R. Leveraging material properties in fluorescence anion sensor arrays: a general approach. *Chemistry—A European Journal*, 2013, 19(26): 8497–8506
21. Sasaki Y, Leclerc É, Hamedpour V, Kubota R, Takizawa S, Sakai Y, Minami T. Simplest chemosensor array for phosphorylated saccharides. *Analytical Chemistry*, 2019, 91(24): 15570–15576
22. Zaubitzer F, Buryak A, Severin K. Cp*Rh-based indicator-displacement assays for the identification of amino sugars and aminoglycosides. *Chemistry—A European Journal*, 2006, 12(14): 3928–3934
23. Palacios M A, Wang Z, Montes V A, Zyryanov G V, Anzenbacher P Jr. Rational design of a minimal size sensor array for metal ion detection. *Journal of the American Chemical Society*, 2008, 130(31): 10307–10314

24. Liang X, Bonizzoni M. Boronic acid-modified poly(amidoamine) dendrimers as sugar-sensing materials in water. *Journal of Materials Chemistry. B, Materials for Biology and Medicine*, 2016, 4(18): 3094–3103
25. Liu C, Wang P, Liu X, Yi X, Zhou Z, Liu D. Supramolecular fluorescent sensor array for simultaneous qualitative and quantitative analysis of quaternary ammonium herbicides. *New Journal of Chemistry*, 2018, 42(21): 17317–17322
26. Yao Z, Feng X, Hong W, Li C, Shi G. A simple approach for the discrimination of nucleotides based on a water-soluble polythiophene derivative. *Chemical Communications*, 2009, 31(31): 4696–4698
27. Maynor M S, Deason T K, Nelson T L, Lavigne J J. Multi-dimensional response analysis towards the detection and identification of soft divalent metal ions. *Supramolecular Chemistry*, 2009, 21(3–4): 310–315
28. Li C, Shi G. Polythiophene-based optical sensors for small molecules. *ACS Applied Materials & Interfaces*, 2013, 5(11): 4503–4510
29. Doré K, Dubus S, Ho H A, Lévesque I, Brunette M, Corbeil G, Boissinot M, Boivin G, Bergeron M G, Boudreau D, Leclerc M. Fluorescent polymeric transducer for the rapid, simple, and specific detection of nucleic acids at the zeptomole level. *Journal of the American Chemical Society*, 2004, 126(13): 4240–4244
30. McCullough R D, Ewbank P C, Loewe R S. Self-assembly and disassembly of regioregular, water soluble polythiophenes: chemoselective ionchromatic sensing in water. *Journal of the American Chemical Society*, 1997, 119(3): 633–634
31. Li C, Numata M, Takeuchi M, Shinkai S. A sensitive colorimetric and fluorescent probe based on a polythiophene derivative for the detection of ATP. *Angewandte Chemie International Edition*, 2005, 44(39): 6371–6374
32. Ho H A, Leclerc M. New colorimetric and fluorometric chemosensor based on a cationic polythiophene derivative for iodide-specific detection. *Journal of the American Chemical Society*, 2003, 125(15): 4412–4413
33. Sasaki Y, Ito S, Zhang Z, Lyu X, Takizawa S, Kubota R, Minami T. Supramolecular sensor for astringent procyanidin C1: fluorescent artificial tongue for wine components. *Chemistry—A European Journal*, 2020, 26(69): 16236–16240
34. Domínguez S E, Meriläinen M, Ääritalo T, Damlin P, Kvarnström C. Effect of alkoxy-spacer length and solvent on diluted solutions of cationic isothiuronium polythiophenes. *RSC Advances*, 2017, 7(13): 7648–7657
35. Minami T, Kubo Y. Fluorescence sensing of phytate in water using an isothiuronium-attached polythiophene. *Chemistry—A Asian Journal*, 2010, 5(3): 605–611
36. An Y, Xiao K, Yao Z, Li C. Conjugated polyelectrolyte based colorimetric array for the discrimination of primary amino acids. *ChemistrySelect*, 2020, 5(18): 5400–5403
37. Liu L, Zhao L, Cheng D, Yao X, Lu Y. Highly selective fluorescence sensing and imaging of ATP using a boronic acid groups-bearing polythiophene derivative. *Polymers*, 2019, 11(7): 1139
38. Pal S, Chatterjee N, Bharadwaj P K. Selectively sensing first-row transition metal ions through fluorescence enhancement. *RSC Advances*, 2014, 4(51): 26585–26620
39. Wang Z, Palacios M A, Anzenbacher P Jr. Fluorescence sensor array for metal ion detection based on various coordination chemistries: general performance and potential application. *Analytical Chemistry*, 2008, 80(19): 7451–7459
40. Xu W, Ren C, Teoh C L, Peng J, Gadre S H, Rhee H W, Lee C L K, Chang Y T. An artificial tongue fluorescent sensor array for identification and quantitation of various heavy metal ions. *Analytical Chemistry*, 2014, 86(17): 8763–8769
41. Smith D G, Sajid N, Rehn S, Chandramohan R, Carney I J, Khan M A, New E J. A library-screening approach for developing a fluorescence sensing array for the detection of metal ions. *Analyst*, 2016, 141(15): 4608–4613
42. Hwang I H, Hong K I, Jeong K S, Jang W D. Carbazole-based molecular tweezers as platforms for the discrimination of heavy metal ions. *RSC Advances*, 2015, 5(2): 1097–1102
43. Sasaki Y, Minamiki T, Tokito S, Minami T. A molecular self-assembled colourimetric chemosensor array for simultaneous detection of metal ions in water. *Chemical Communications*, 2017, 53(49): 6561–6564
44. Inoue M B, Velazquez E F, Inoue M. One-step chemical synthesis of doped polythiophene by use of copper(II) perchlorate as an oxidant. *Synthetic Metals*, 1988, 24(3): 223–229
45. Minami T, Kubo Y. Selective anion-induced helical aggregation of chiral amphiphilic polythiophenes with isothiuronium-appended pendants. *Supramolecular Chemistry*, 2011, 23(1–2): 13–18
46. Derakhshesh M, Gray M R, Dechaine G P. Dispersion of asphaltene nanoaggregates and the role of rayleigh scattering in the absorption of visible electromagnetic radiation by these nanoaggregates. *Energy & Fuels*, 2013, 27(2): 680–693
47. Rasmussen S C, Evenson S J, McCausland C B. Fluorescent thiophene-based materials and their outlook for emissive applications. *Chemical Communications*, 2015, 51(22): 4528–4543
48. Wang X, Zhao J, Guo C, Pei M, Zhang G. Simple hydrazide-based fluorescent sensors for highly sensitive and selective optical signaling of Cu^{2+} and Hg^{2+} in aqueous solution. *Sensors and Actuators. B, Chemical*, 2014, 193: 157–165
49. Keizer J. Nonlinear fluorescence quenching and the origin of positive curvature in stern-volmer plots. *Journal of the American Chemical Society*, 1983, 105(6): 1494–1498
50. You J, Kim J, Park T, Kim B, Kim E. Highly fluorescent conjugated polyelectrolyte nanostructures: synthesis, self-assembly, and Al^{3+} ion sensing. *Advanced Functional Materials*, 2012, 22(7): 1417–1424
51. Chen Y, Pu K Y, Fan Q L, Qi X Y, Huang Y Q, Lu X M, Huang W. Water-soluble anionic conjugated polymers for metal ion sensing: effect of interchain aggregation. *Journal of Polymer Science. Part A, Polymer Chemistry*, 2009, 47(19): 5057–5067
52. Bala T, Prasad B L V, Sastry M, Kahaly M U, Waghmare U V. Interaction of different metal ions with carboxylic acid group: a quantitative study. *Journal of Physical Chemistry A*, 2007, 111(28): 6183–6190
53. Miller J N, Miller J C. *Statistics and Chemometrics for Analytical Chemistry*. 7th ed. Essex: Pearson Higher Education, 2018
54. Wolfbeis O S. *Materials for fluorescence-based optical chemical*

- sensors. *Journal of Materials Chemistry*, 2005, 15(27-28): 2657–2669
55. Anzenbacher P Jr, Liu Y L, Kozelkova M E. Hydrophilic polymer matrices in optical array sensing. *Current Opinion in Chemical Biology*, 2010, 14(6): 693–704
56. Guo T R, Zhang G P, Zhang Y H. Physiological changes in barley plants under combined toxicity of aluminum, copper and cadmium. *Colloids and Surfaces. B, Biointerfaces*, 2007, 57(2): 182–188